Dielectric and conductivity spectroscopy of $Li_{1-x}Ni_{1+x}O_2$ in the range of 10–10^{10} Hz: polaron hopping

2002 J. Phys.: Condens. Matter 14 6917

(http://iopscience.iop.org/0953-8984/14/28/303)

INSTITUTE OF PHYSICS PUBLISHING JOURNAL OF PHYSICS: CONDENSED MATTER

J. Phys.: Condens. Matter **14** (2002) 6917–6930 PII: S0953-8984(02)35425-0

Dielectric and conductivity spectroscopy of $Li_{1-x}Ni_{1+x}O_2$ in the range of 10–10^{10} Hz: polaron hopping

J C Badot[1,3], V Bianchi[1], N Baffier[1] and N Belhadj-Tahar[2]

[1] Ecole Nationale Supérieure de Chimie de Paris (ENSCP), Laboratoire de Chimie Appliquée de l'Etat Solide, UMR CNRS 7574, 11 rue P et M Curie, 75231 Paris Cedex 05, France
[2] Laboratoire de Génie Electrique de Paris, CNRS–Paris VI–Paris XI, Supélec, Plateau de Moulon, 91192 Gif-sur-Yvette Cedex, France

E-mail: badot@ext.jussieu.fr

Received 3 April 2002
Published 5 July 2002
Online at stacks.iop.org/JPhysCM/14/6917

Abstract

Dielectric and conductivity spectra of the compound $Li_{1-x}Ni_{1+x}O_2$ ($x = 0.03$) are reported and analysed. The spectra were recorded for compacted powders within the broad frequency range 10–10^{10} Hz at temperatures varying between 210 and 300 K. The evolution of the spectra of the sample with respect to the damage under air allows us to define two regimes: the first one is an interfacial regime and the second a bulk regime. The frequency of crossover (ν_{co}) between the two regimes lies in the interval 1×10^9 and 2×10^9 Hz at room temperature. At frequencies below ν_{co}, the spectral analysis shows dielectric relaxations due to interfacial polarization phenomena in the sample. The complex resistivity plots (for $\nu < \nu_{co}$) allowed the determination of the dc conductivity of $Li_{1-x}Ni_{1+x}O_2$ versus temperature. At frequencies greater than ν_{co}, one dielectric relaxation corresponding to small-polaron hopping has been observed. The corresponding relaxation frequency is thermally activated with an activation energy of 0.15–0.16 eV and a pre-exponential factor $\nu_0 \approx 3 \times 10^{12}$–$4 \times 10^{12}$ Hz, which is of the order of the longitudinal-optical-phonon frequency ν_{LO}. The conduction behaviour is interpreted in terms of hopping of small polarons (holes) on an oxygen network.

1. Introduction

The recent interest in studying the physical [1–4] properties of $LiNiO_2$ was stimulated by its promise as regards use as a cathodic material in advanced rechargeable lithium batteries [5–8]. The mixed oxide $LiNiO_2$ exhibits a layered rhombohedral structure with $R\bar{3}m$ space group.

[3] Author to whom any correspondence should be addressed.

0953-8984/02/286917+14$30.00

The ideal structure of $LiNiO_2$ consists of successive layers of lithium, oxygen and nickel ions. The hexagonal lattice parameters are $a = 2.88$ Å and $c = 14.2$ Å. The oxygen ions (6c sites) form a close-packed stacking. Lithium and nickel ions are respectively in 3a and 3b octahedral sites. Since the lithium deficiency x deviates from zero, the exact formula of the compound is $Li_{1-x}Ni_{1+x}O_2$, with x nickel ions in excess located in lithium layers (3a sites); this can strongly impede Li^+-ion diffusion during electrochemical cycles. Some conflicting investigations were devoted to the electronic structure of these compounds. In the simple ionic model, Ni^{3+} ions are expected in $LiNiO_2$ since the electronic holes reside on Ni. However, recent O 1s absorption spectra and band structure calculations have shown that the presence of Li^+ ions leads to the formation of an impurity acceptor O 2p band [9–14]. The hole-compensating Li^+ charge in $Li_{1-x}Ni_{1+x}O_2$ has an O 2p character rather than an Ni 3d character. Consequently, it follows that holes are most probably on the oxygen atoms of the $[NiO_6]$ units. Hence, $Li_{1-x}Ni_{1+x}O_2$ would be in the negative-charge-transfer regime whose ground state is described by $Ni^{2+}(O_6)^{-11}$ or Ni^{2+} L (L = ligand hole) ($S = 1/2$) rather than $Ni^{3+}(O_6)^{-12}$ ($S = 1/2$) [2, 15]. The O 2p holes have a very large antiferromagnetic exchange interaction with neighbouring $Ni^{2+}d^8$ spins, which makes them appear like low-spin Ni^{3+} states in macroscopic magnetic measurements, Ni^{3+} being equivalent to the Ni^{2+} L complex. Harrison *et al* [14] have suggested that the hole states are small polarons, whose binding energy would be about 0.27 eV. Localized states of this type have also been evidenced from calculations [16] and dielectric measurements on NiO [17].

The study of electrical transport properties becomes complicated since $LiNiO_2$ can only be made in powder form and is not stable in air, owing to the formation of an insulating phase Li_2CO_3. So, the conductivity measurements by usual dc or low-frequency techniques, which have shown the semiconducting behaviour of $LiNiO_2$, cannot give any information on the electrical transport properties [18, 19] owing to the complexity of the microstructures in compounds of this type: the existence of grain boundary barriers and of agglomeration of powder particles in some cases. Strong frequency dependence of the permittivity in the low-frequency region was noted in many polycrystalline samples which consist of semiconducting grains (single crystals) separated by quasi-insulating grain boundary layers [20–22]. In this scheme, the central core (bulk) of the grains is surrounded by a quasi-insulating depletion or accumulation layer. In other words, the grains are polarized by the accumulation of charge carriers on their boundaries, under the action of an electric field. So, the grains can be assimilated to 'giant dipoles' giving rise to dielectric relaxation, whose relaxation frequency ν_g is inversely proportional to the size and the resistivity of the grain [20, 23]. In this case, the relaxation time $\tau = (2\pi\nu_g)^{-1}$ corresponds to the transit time of the charge carriers in the grains.

For frequencies far above ν_g, the dielectric spectra are determined by the bulk properties of the grains in which charge motions can involve frequency-dependent conductivity and permittivity. Subsequently, we will only consider charge motion in some semiconducting crystalline compounds in which small-polaron hopping occurs on sites distributed regularly. Odagaki *et al* [24] have studied the stochastic transport in one-dimensional hopping conductors (electronic or ionic), in which two or more kinds of hopping rate are distributed regularly. If we consider a double-well system between two finite potential barriers, the model of Odagaki *et al* [24] predicts one Debye dielectric relaxation. According to Fröhlich [25] and Bosman and van Daal [17], the Debye dielectric relaxation can only occur with small-polaron formation in low-mobility semiconductors [26–38]. As the dielectric relaxation is the result of an electric dipole reorientation, we have to consider only local (confined) hopping of small polarons around an immobile ion [17, 21, 29] or in a double-well system between two finite potential barriers [24, 30]. The dielectric relaxation time corresponds to the hopping time of the charge and is generally thermally activated.

The dielectric relaxations are generally described by the Havriliak–Negami (HN) function [31] of the complex permittivity $\varepsilon(\nu)$:

$$\varepsilon(\nu) = \varepsilon_{hf} + \frac{\varepsilon_{lf} - \varepsilon_{hf}}{(1 + (\mathrm{i}\, 2\pi\, \nu\tau)^{1-\alpha})^{\beta}} \tag{1}$$

where ε_{lf} and ε_{hf} are respectively the low-and high-frequency limits of the permittivity; τ is the relaxation time. The parameters α and β range between 0 and 1 and determine the degree of deviation from the ideal Debye response for which $\alpha = 0$ and $\beta = 1$. The dielectric relaxation due to the presence of the grain boundaries is often fitted by the Cole–Cole (CC) function [32] for which $\beta = 1$. Furthermore, Jonscher *et al* [33] have suggested that the charge hopping confined in a double well gives rise to a 'near-Debye' response, which can be described by a CC function with $\alpha < 0.3$.

As a result, the dielectric and the conductivity spectra may be described in terms of two regimes with respect to the frequency: an interfacial (surface) regime and a bulk regime. Between these two regimes, we define a frequency of crossover ν_{co} beyond which the electrical properties are only determined by the bulk properties of the grains, i.e. the interfacial (grain boundary) effects on the permittivity and the conductivity are negligible. The crossover frequency ν_{co} is thus higher than the relaxation frequency ν_g of the reorientation of the grain boundary polarization. At frequencies $\nu \ll \nu_{co}$, the permittivity and the conductivity are only defined by the interfacial effects.

In previous studies [21, 22], we have shown that the dielectric properties between 10 and 10^{10} Hz can provide very important information regarding small-polaron dynamics in powdered compounds. In the present work, we report the first detailed study concerning the dielectric and conductivity spectroscopy of $Li_{1-x}Ni_{1+x}O_2$ compound ($x = 0.03$) from 10 to 10^{10} Hz. The sample was kept under air in order to form an insulating phase Li_2CO_3. The influence of the treatment will permit us to determine the bulk and interfacial regimes of the dielectric and conductivity spectra. Hence, the study of local motions of charge (holes) will also be discussed in order to explain the electronic conductivity of $Li_{1-x}Ni_{1+x}O_2$ with respect to the temperature.

2. Experimental procedures

2.1. Sample synthesis and structure

In the present study, the compound $Li_{1-x}Ni_{1+x}O_2$ (hereafter called LNOA) was prepared by a classical method consisting of the solid-state reaction described by Lecerf *et al* [34]. The powder was heated at 700 °C under an efficient oxygen flow for 5–24 h. The lithium deficiency $x = 0.03$ was determined by Rietveld profile fitting of x-ray diffraction data ($\lambda_{\mathrm{Co\,K}\alpha_1}$) and verified by magnetic measurements [8]. The coherence lengths ξ of the diffracting domains in powder particles, determined from x-ray diffraction linewidths, were found to range between 130 and 180 nm [8]. The ξ-values are lower than the average particle sizes which are 200 and 2000 nm for the sample. Hence, the powder particles can be considered as small polycrystals constituted by some monocrystalline domains (or grains). The microstructure can be described by two types of interface, i.e. particle–particle and grain–grain.

The sample must be kept under vacuum or argon to avoid degradation. However, the formation of a small quantity of lithium carbonate (Li_2CO_3) was evidenced by x-ray diffraction (figure 1), when the sample was left for a few weeks in air. Lithium carbonate is preferentially formed on particle and grain surfaces.

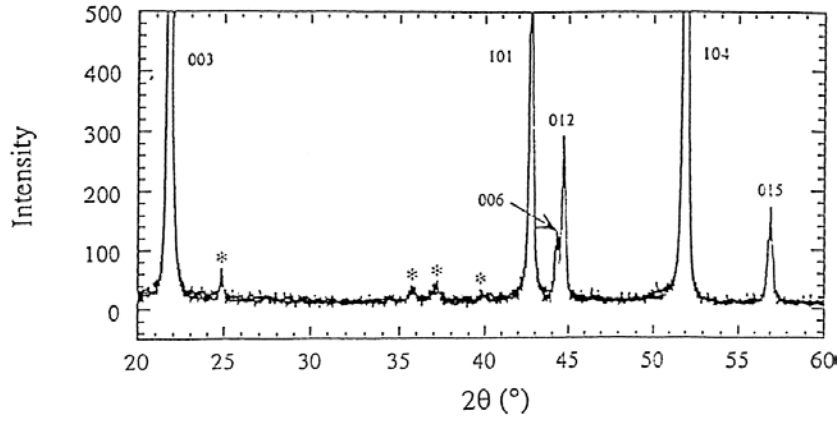

Figure 1. The x-ray diffraction pattern for $Li_{1-x}Ni_{1+x}O_2$ damaged under air. Evidence of diffraction peaks (*) corresponding to Li_2CO_3.

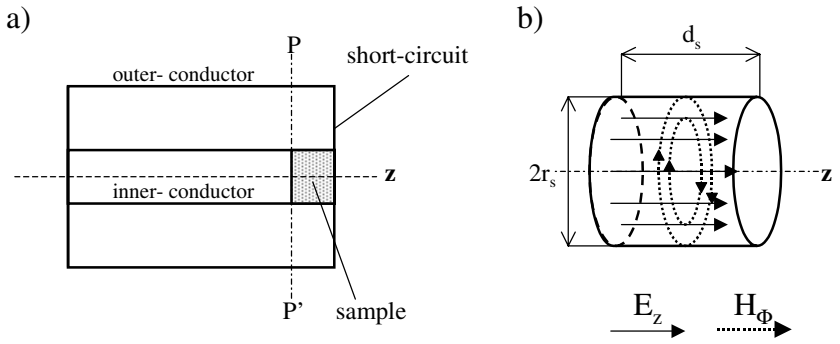

Figure 2. The coaxial line (APC7 standard) used in the frequency range 10–10^{10} Hz [21, 39]: (a) the sample fills the gap between the inner conductor and a short-circuit; (b) the electromagnetic field distribution in the sample.

2.2. Conductivity and dielectric measurements

Complex resistivity, conductivity and permittivity measurements were performed between 220 and 300 K (under N_2 flux) over a broad frequency range from 10 to 10^{10} Hz, using simultaneously two network analysers (HP 8751 and HP 8510). The experimental device, which has been fully described in previous papers [21, 35–39], consists of a coaxial cell (APC7 standard) in which the cylindrically shaped sample fills the gap between the inner conductor and a short-circuit (figure 2(a)). The sample and the inner conductor axis (z-axis) are identical. The sample (about 15 mg) was compacted into cylindrical pellets under a uniaxial pressure equal to at most 7 kPa. The sample had the same radius r_s as the inner conductor (i.e. 1.5 mm) and its thickness d_s was about 1 mm. The sample porosities are not so different since they were evaluated as between 33 and 35%. The sample front faces were covered with a silver layer to ensure good electrical contacts with the inner conductor on one hand and with the short-circuit on the other.

After an appropriate calibration of the network analysers, the sample admittance Y_s is computed from measurements of the complex reflection coefficient in the reference plane PP′. Hence, the knowledge of Y_s allows one to determine the complex permittivity (in fact, the

relative permittivity) $\varepsilon(\nu)$ of the sample according to

$$Y_s = \mathrm{i}\frac{k_s r_s}{\nu\mu_0 d_s}\frac{J_1(k_s r_s)}{J_0(k_s r_s)} \tag{2}$$

where $\mathrm{i} = (-1)^{1/2}$, $k_0 = 2\pi\nu/c$ ($c = 3 \times 10^8$ m s^{-1}), $k_s = k_0(\varepsilon(\nu))^{1/2}$, μ_0 is the free-space permeability. r_s and d_s are the radius and the thickness of the sample, respectively. J_0 and J_1 are zero- and first-order Bessel functions of the first kind, respectively. Expression (2) is only applicable for $d_s < \lambda_s/2$, where λ_s is the wavelength in the sample. In this case, a radial propagation is present with only the axial component E_z of the electric field and the azimuthal component H_ϕ of the magnetic field in the sample (figure 2(b)).

The permittivity $\varepsilon(\nu) = \varepsilon'(\nu) - \mathrm{i}\varepsilon''(\nu)$, where the real part $\varepsilon'(\nu)$ and imaginary part $\varepsilon''(\nu)$ have been calculated using an iterative method derived from the gradient method [40]. So, knowledge of the permittivity allows the calculation of the complex conductivity $\sigma(\nu) = \mathrm{i}\,2\pi\nu\varepsilon_0\varepsilon(\nu)$. It is also possible to obtain the real part $\rho'(\nu)$ and imaginary part $\rho''(\nu)$ of the complex resistivity $\rho(\nu) = (\sigma(\nu))^{-1}$. The dielectric spectra were made up from about 600 measurements with an accuracy of 3–5%, over the whole frequency range. The coaxial cell containing the sample can only be used in the temperature range 180–450 K.

3. Results and discussion

3.1. Frequency-dependent permittivity and conductivity

Figure 3 (curves A1) shows the frequency dependence of the real parts of the conductivity and permittivity of LNOA at room temperature. For frequency below 3×10^9 Hz, the conductivity of LNOA is independent of the frequency (curve A1 in figure 3(a)) and is equal to the dc conductivity of the sample pellets in the low-frequency range ($\nu < 1 \times 10^4$ Hz). Such a behaviour corresponds to a ν^{-1} frequency response of the dielectric losses (imaginary part of ε). The real part $\varepsilon'(\nu)$ of the complex permittivity shows a low-frequency dispersion (curve A1 in figure 3(b)), which can be approximated by a straight line with a slope close to -1. Such a behaviour corresponds to a ν^{-1} frequency response in the low-frequency domain ($\nu < 2 \times 10^3$ Hz). Furthermore, $\varepsilon'(\nu)$ rises to high values between 10^5 and 10^6 at 10 Hz, which indicates a high capacitive effect of the semiconductor–metal junction. The semiconductor–metal junction is a partially blocking and ohmic contact, giving rise to the existence of a limited charge flow (resistive part) and a polarization (capacitive part) at the junction. In the low-frequency domain, the electrical equivalent circuit of the system can be schematized as two parallel combinations of resistance and capacitance in series: the first one is associated with the sample bulk and the other with the interfacial region. The dielectric response is described by the Debye relaxation model, for which ε' and ε'' follow respectively ν^{-2} and ν^{-1} frequency responses for frequencies above the relaxation frequency. In this case the dielectric losses ε'' are due to the dc conductivity of the sample. However, the Debye model cannot explain the experimental ν^{-1} frequency response of the real part ε'. As the sample surfaces are rough, the existence of a distribution of interfacial resistances and capacitances gives rise to a distribution of relaxation times involving a dielectric response described by the CC expression. In this model, ε' and ε'' are proportional to $\nu^{\alpha-1}$ for frequencies above the relaxation frequency (or loss-peak frequency). Such a behaviour corresponds to the Jonscher empirical model ('universal dielectric response') [41], which describes the low-frequency dispersion in materials. The ν^{-1} experimental low-frequency response of ε', which has often been observed for various solids, is a consequence of a distribution of relaxation times with a near-zero value of the parameter α ($\alpha \ll 1$) (see also section 3.2).

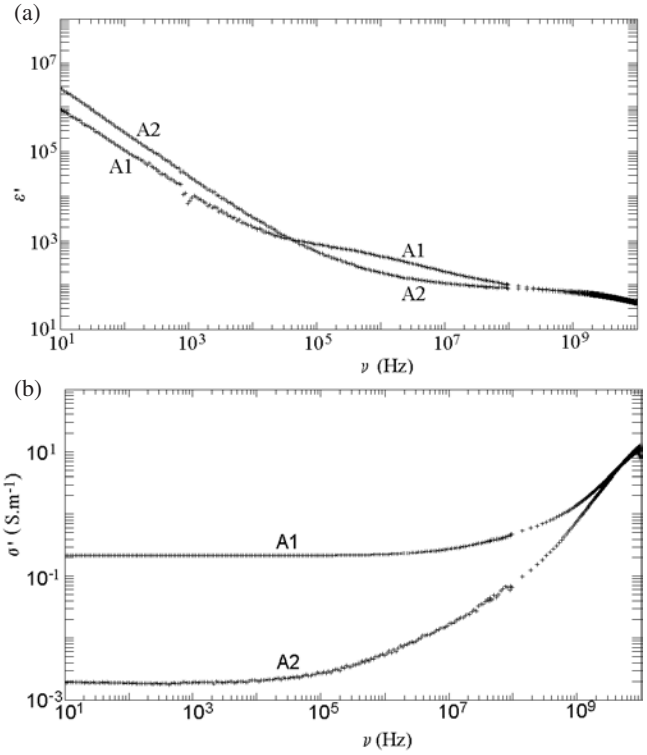

Figure 3. (a), (b) Real parts of the conductivity σ' and permittivity ε' as functions of frequency ν at room temperature for the compound $Li_{0.97}Ni_{1.03}O_2$. The curves A1 correspond to the sample LNOA (pure compound) and the curves A2 to the sample LNOAD (LNOA damaged after a few weeks under air), which contains a low content of Li_2CO_3.

To study the effect of the damaging in air on the electrical properties of the sample, frequency-dependent conductivity (real part) and permittivity (real and imaginary parts) have been measured for the same LNOA sample ($Li_{0.97}Ni_{1.03}O_2$) in the following way: first, immediately after conservation under vacuum (curves A1, figure 3) and after a few weeks under air (curves A2, figure 3). After this transformation, LNOA will hereafter be called LNOAD. Figure 3(a) shows that the low-frequency conductivity strongly decreased by about two orders of magnitude as the sample was damaged in air. This phenomenon is due to the formation of an insulating layer of Li_2CO_3 on the grain boundaries, since the high-frequency conductivity (for $\nu > 1 \times 10^9$ Hz) is not modified and is thus intrinsic to the bulk of the grains. The evolution of the spectra with respect to the formation of Li_2CO_3 during the damaging has provided evidence of two regimes: the first one is an interfacial (low-frequency) regime and the second a bulk (high-frequency) regime. The frequency of crossover, ν_{co}, between the two regimes lies in the frequency range 10^9 to 3×10^9 Hz at room temperature. The crossover frequency ν_{co} becomes lower as the temperature decreases ($\nu_{co} \approx 10^8$ Hz at 220 K), which broadens the frequency range of the bulk regime. The dielectric relaxations, which occur for frequencies below ν_{co}, are thus only due to the existence of interfacial polarizations under an applied electric field.

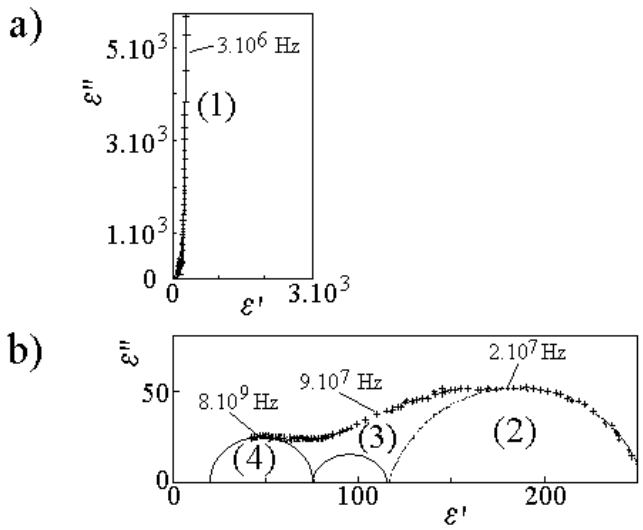

Figure 4. (a) A CC plot of the imaginary part $\varepsilon''(\nu)$ versus the real part $\varepsilon'(\nu)$ of the permittivity $\varepsilon(\nu)$ at room temperature for LNOA; (b) relaxation domains 2, 3 and 4 obtained after subtracting respectively the contributions of the domains 1, 2 and 3.

3.2. Evidence for and assignment of dielectric relaxations

For dielectric spectroscopy, the main problem lies in the assignment of the dielectric relaxations in granular materials. A first criterion is the knowledge of the microstructure and the crystalline structure of the compound, obtained using scanning electron microscopy and x-ray diffraction. A second criterion is the determination of the nature of the different charge carriers which can be evidenced by the knowledge of the electronic structure and by spectroscopic studies. A third criterion is the knowledge of the chemical stability of the compound, to avoid some erroneous interpretations. As the possible dielectric relaxations are not clearly shown in frequency-dependent representations, it is more suitable to use Cole–Cole (CC) plots in order to get an easier decomposition of the dielectric spectra. To provide evidence for the dielectric relaxations, we employed a procedure of decomposition of the CC plots, which has been fully described elsewhere [21, 37–39].

Figure 4(a) shows the entire CC plot (from 10 to 10^{10} Hz) of LNOA at room temperature. The first dispersion domain (domain 1) is fitted between 10 and 10^3 Hz with a good precision by a quasi-vertical straight line, which corresponds to a $\nu^{\alpha-1}$ frequency response of the complex permittivity with the exponent $\alpha = 3 \times 10^{-3}$. This response is the high-frequency part of a 'quasi-Debye' relaxation due to the silver/sample interface as shown in section 3.1. Upon subtracting this low-frequency contribution, a graph is obtained (figure 4(b)). For frequency below 3×10^7 Hz, the graph of figure 4(b) is well fitted by the HN function with $\alpha \approx 0.14$, $\beta \approx 1$ and a relaxation frequency $\nu_2 \approx 2 \times 10^7$ Hz at room temperature. This second dispersion domain (domain 2) is thus described by a CC function represented by a circular arc (figure 4(b)). By the same procedure, we obtain unambiguously two other relaxation domains (domains 3 and 4), which are also well fitted by CC functions with α respectively equal to 0.18 and 0.14 and described by circular arcs (figure 4(b)). The last two dispersion domains 3 and 4 have respective relaxation frequencies $\nu_3 \approx 2 \times 10^8$ Hz and $\nu_4 \approx 8 \times 10^9$ Hz at room temperature. Since each fit has been made over 20–100 measurement points (each point corresponding to a value of ε or σ at a fixed frequency), the decomposition procedure determines unequivocally the

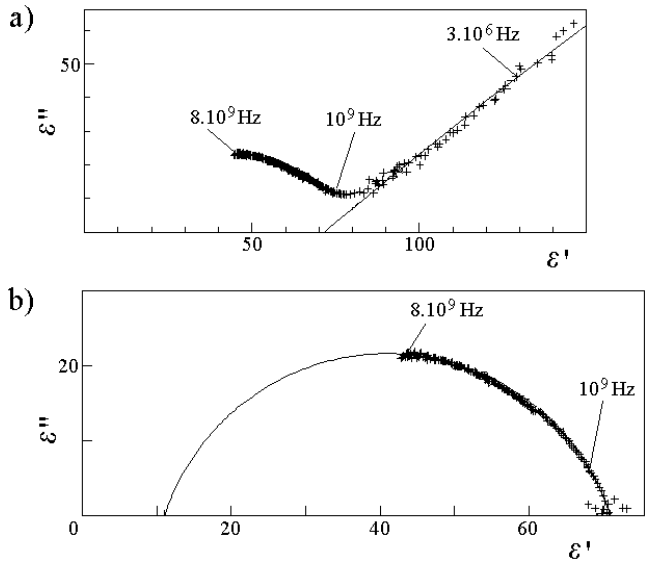

Figure 5. (a) A CC plot of the imaginary part $\varepsilon''(\nu)$ versus the real part $\varepsilon'(\nu)$ of the permittivity $\varepsilon(\nu)$ at room temperature for LNOAD (LNOA damaged after a few weeks under air); (b) the second dispersion (relaxation) domain after subtracting the low-frequency domain.

different parameters with a reasonable precision. As the temperature and relaxation frequency decrease together, the last relaxation domain 4 is determined by more than 100 measurement points.

Figure 5 shows the entire CC plot of LNOAD (LNOA damaged under air over a few weeks). In this case, we observe only two dispersion domains obtained unequivocally by the same decomposition procedure. For the low-frequency domain, which is fitted by a straight line from 10^6 to 10^9 Hz, the real and imaginary parts of the permittivity ε exhibit a $\nu^{0.36}$ frequency response, the corresponding ac conductivity varying as $\nu^{0.64}$. The dc conductivity of the LNOAD would correspond to the surface conductivity of the Li_2CO_3 layer which wraps the powder particles. This phenomenon would be due to the lithium-ion surface diffusion, which would explain the important value of the ionic conductivity around 2×10^{-5} S cm^{-1} at room temperature. The fractional power law for the conductivity can be explaining by various theories devoted to ionic conductors [42, 43]. The high-frequency domain is well fitted by 100–150 points and described by a circular arc (i.e. CC function). This domain corresponds to a dielectric relaxation whose strength, relaxation frequency and α-parameter are equal to those of domain 4 of LNOA.

The dielectric relaxations domains 2 and 3, which have relaxation frequencies below the crossover frequency $\nu_{co} \approx 10^9$ Hz, are then attributed to the interfacial polarizations in LNOA. To this end, evidence was given in section 2.1 of the existence of two types of interface in LNOA. Hence, as the relaxation frequencies are proportional to the inverse size of the particles or grains (see expression (1)), we may assign the relaxation domains 2 and 3 to particle and grain boundary polarizations respectively.

The CC plots have also revealed a relaxation domain 4, which is intrinsic to the grain bulk, since it corresponds to the high-frequency part of dielectric spectra (frequency higher than 10^9 Hz). This dielectric relaxation is due to charge carriers hopping in the $Li_{1-x}Ni_{1+x}O_2$ lattice.

3.3. Electrical properties of the bulk: small-polaron hopping and dc conductivity

As the crystalline compound $Li_{1-x}Ni_{1+x}O_2$ contains lithium ions in layers of the structure, the observed relaxation domain 4 could be only due either to lithium-ion hopping or to small-polaron hopping. Since the 3a sites are all occupied by $(1-x)$ lithium and x nickel ions [5–8], the lithium motion is thus hindered. Consequently, the relaxation domain 4 is associated with a small-polaron (hole) hopping on oxygen atoms. However, the small-polaron hopping can be either adiabatic or non-adiabatic [26, 27, 44–46]. In the former case, the (adiabatic) hopping frequency follows an Arrhenius law:

$$\nu_h = \nu_{LO} \exp(-W_h/kT) \tag{3}$$

where W_h is the activation energy and ν_{LO} is the longitudinal-optical-phonon frequency ($\nu_{LO} \approx 10^{12}$ to 10^{13} Hz). In the latter case, the (non-adiabatic) hopping frequency is determined by the following expression [26, 27, 44–46]:

$$\nu_h = \frac{\pi^{1/2} J^2}{2h(W_h kT)^{1/2}} \exp(-W_h/kT) \tag{4}$$

where h is the Planck constant and J is the integral for electron transfer between neighbouring sites. The hopping regime of the small polarons is generally observed in the high-temperature region, i.e. for $T > h\nu_{LO}/2$ [45]. The relaxation frequency ν_4 follows the two expressions (3) and (4), for which straight lines are obtained by plotting $\log \nu_4$ versus $1/T$ (figure 6(a)) and $\log(\nu_4 T^{1/2})$ versus $1/T$ (figure 6(b)). The plot analysis of figure 6(a) yields an activation energy $W_h = 0.15$ eV and a prefactor $\nu_0 \approx 3 \times 10^{12}$ Hz of the order of the longitudinal-optical-phonon frequencies. The plot analysis of figure 6(b) yields an activation energy $W_h = 0.16$ eV and $J \approx 0.035$ eV. The prefactor of the expression (4) has a very slow variation with respect to the temperature, i.e. $\nu_0 \approx 4 \times 10^{12}$ Hz in the present experimental temperature range. The preliminary data analysed herein are not sufficiently precise for distinguishing between the two types of hopping. However, a non-adiabatic small-polaron conduction needs two conditions to be fulfilled [26, 27, 44–46]:

$$J < 4Wh \tag{5a}$$

$$J < (h\nu_{LO})^{1/2}(W_h kT)^{1/4}. \tag{5b}$$

The first inequality (5*a*) is obeyed since $W_h = 0.16$ eV. Assuming that $\nu_{LO} = 10^{12}$ to 10^{13} Hz and $T = 220$ K, the value of $(h\nu_{LO})^{1/2}(W_h kT)^{1/4}$ is between 0.015 and 0.048 eV which is actually similar to the value of $J = 0.035$ eV. As a result, we cannot describe the present experimental results in terms of non-adiabatic small-polaron hopping until the experimental value of ν_{LO} is measured. Despite the ambiguity, the value of the polaron binding energy $W_p \approx 2W_h = 0.30$ or 0.32 eV is in good agreement with the value ($W_p \approx 0.27$ eV) calculated by Harrison *et al* [14].

The dc conductivity (i.e. grain bulk dc conductivity) σ_{ge} of LNOA was obtained by the complex impedance method in the low-frequency range ($\nu < 10^9$ Hz). Figure 7 shows the typical complex resistivity diagram, $\rho'' = f(\rho')$, at room temperature. Resistivity relaxation domains, obtained by successive subtractions as in the CC plots, are represented by circular arcs. These relaxations have the same origin as those of the CC plots: domains 2–4. However, the low-frequency domain (domain 1) has been reduced to a point since $\rho' \approx \sigma_{dc}^{-1}$ and $\rho'' \approx 0$. The circular arc (domain 4) is due to contact resistances and capacitances between the grains. It is then possible to obtain the bulk dc resistivity ρ_{ge} (or dc conductivity $\sigma_{ge} = \rho_{ge}^{-1}$) of the grains from the intersection of the high-frequency part of the circular arc with the real axis (ρ'-axis). The value of the dc conductivity is $\sigma_{ge} = 0.10$ S cm^{-1} at room temperature. The temperature dependence of σ_{ge} is ruled by the two expressions $\sigma_{ge}T = D_{ge} \exp(-W_\sigma/kT)$

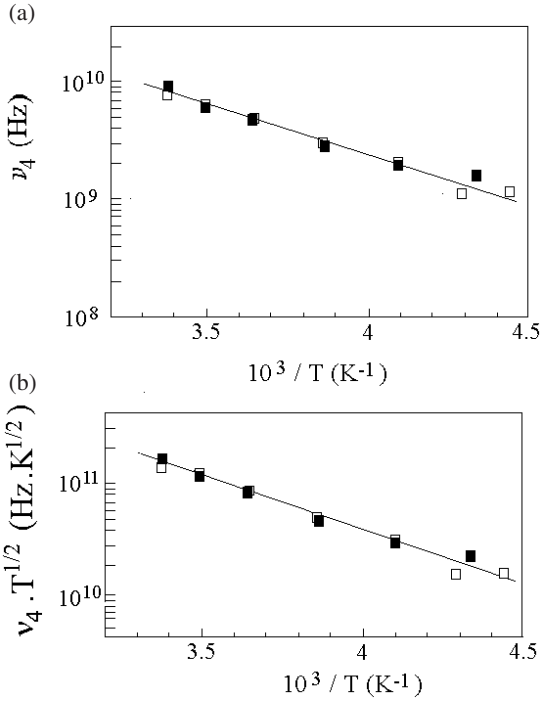

Figure 6. Relaxation frequency ν_4 of domain 4 and hopping frequency of the small polaron as a function of inverse temperature T^{-1} for the samples LNOA (□) and LNOAD (■). (a) The Arrhenius relation ν_4 versus T^{-1}; (b) the Arrhenius relation $\nu_4 T^{1/2}$ versus T^{-1}.

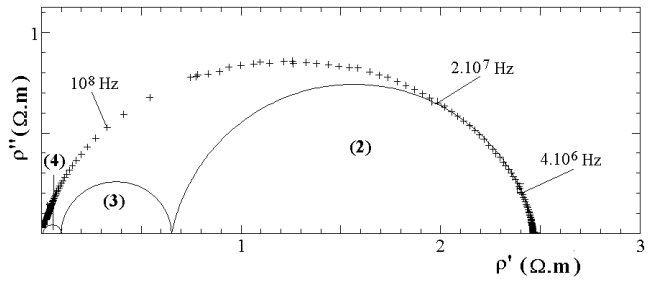

Figure 7. Plots of the imaginary part $\rho''(\nu)$ versus the real part $\rho'(\nu)$ of the complex resistivity for the compound LNOA at 300 K.

(figure 8(a)) and $\sigma_{ge} T^{3/2} = D_{ge} \exp(-W_\sigma / kT)$ (figure 8(b)) for adiabatic and non-adiabatic hopping [26, 27, 44–46] respectively. In the former case, we obtain an activation energy $W_\sigma \approx 0.19$–0.20 eV. In the latter case, the result is similar, since the activation energy is $W_\sigma \approx 0.20$–0.21 eV.

As the sample is porous, σ_{ge} is equivalent to the conductivity of an effective medium which consists of a continuous medium $Li_{1-x}Ni_{1+x}O_2$ which embeds the pores. Percolation and general effective medium theories [47, 48] describe how to calculate the conductivity of a sample consisting of a conductive and an insulating phase. The experimental value of the dc

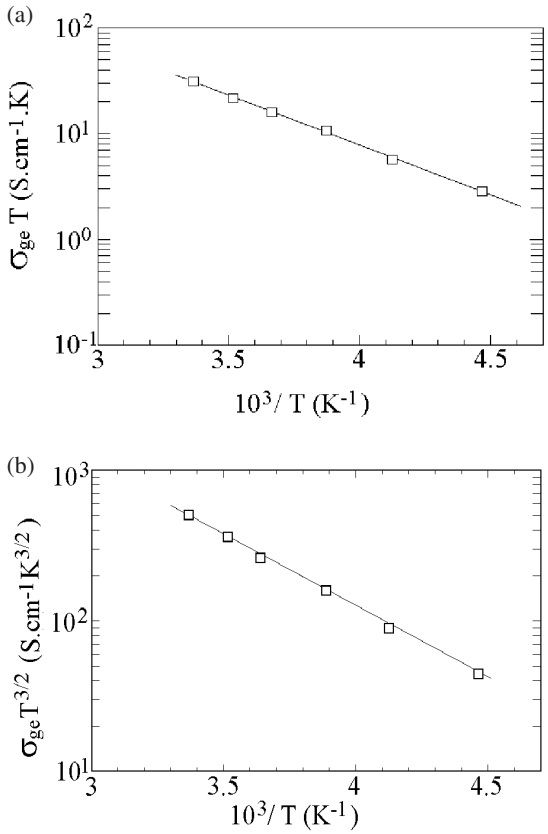

Figure 8. Bulk dc conductivity σ_{ge} as a function of inverse temperature T^{-1} for the sample LNOA. (a) The Arrhenius relation $\sigma_{ge}T$ versus T^{-1}; (b) the Arrhenius relation $\sigma_{ge}T^{3/2}$ versus T^{-1}.

conductivity σ_{ge} can be compared to the value for a hypothetical compact medium σ_g:

$$\frac{\sigma_{ge}}{\sigma_g} = \left[\frac{\phi - \phi_c}{1 - \phi_c}\right]^u \tag{6}$$

where ϕ is the volume fraction of the conductive phase, ϕ_c is the critical percolation threshold and u is a critical exponent. Unfortunately, it is not possible to have access to a wide range of porosity values which would allow us to determine exactly both parameters ϕ_c and u. However, ϕ_c is between 0.10 and 0.40 and u between 1.65 and 2 for 3D systems. Using these values and considering sample porosity $p = (1 - \phi)$ between 33 and 35%, we therefore have $(\sigma_g/\sigma_{ge}) = 2.5$–5.8. The bulk dc conductivity σ_g of the grains is an average value for all possible crystalline orientations since the grains are randomly oriented. The room temperature mobility is thus very low and is at most equal to 10^{-4} cm^2 V^{-1} s^{-1}, which supports the suggestion of small-polaron character for the charge carriers (holes). The activation energy W_σ of the conductivity is higher than the activation energy ($W_h \approx 0.15$ or 0.16 eV) of the relaxation frequency ν_4. As the population of the (holes) small polarons is high ($n > 10^{28}$ m^{-3}), the difference $\Delta W = W_\sigma - W_h$ explains why the relaxation domain 4 arises from a bounced-back effect involving a forward–backward hopping of the (holes) small polarons. The bounced-back effect arises from repulsive coulombic interactions between the neighbouring (hole) polarons.

This phenomenon corresponds to a confined charge hopping between large barriers. A large barrier can be created whenever one small polaron is located in its site for a while; then it becomes blocking for the motion of another small polaron which hops towards its vicinity. In the case of the forward hopping, the charge leaves a site for a neighbouring one, with an activation energy corresponding to that of the dc conductivity. The forward–backward hopping is equivalent to a reorientation of an electric dipole with a dipole moment $m = ea$, where a is the hopping distance and $e = 1.6 \times 10^{-19}$ C. The activation energy of the relaxation process is the same as for the backward hopping. In this way, the splitting of the energy levels ($\Delta W \approx 0.04$–0.05 eV) representing the dipole is higher than kT. Using Einstein's relation, the small-polaron conductivity [45, 49] in the hopping regime is found to be

$$\sigma_{ab} = \frac{Nf(1-f)(ea)^2}{kT} 2\pi \nu_0 \exp\left(-\frac{W_\sigma}{kT}\right) \tag{7}$$

where ν_0, N and f are respectively the attempt frequency, the concentration of lattice sites and the occupation ratio of an oxygen site. For the $Li_{1-x}Ni_{1+x}O_2$ ($x = 0.03$) compound, $f = (1-x)/2 \approx 1/2$ as $x \ll 1$. Assuming that $a = 2.88$ Å, $N \approx 5.88 \times 10^{22}$ cm^{-3}, $\nu_0 = 3 \times 10^{12}$–4×10^{12} Hz, $W_\sigma = 0.19$–0.21 eV and $f \approx 1/2$, it is found from expression (7) that the conductivity is $\sigma_{ab} \approx 0.40$–1.17 S cm^{-1} at room temperature. If the conductivity along the c-axis, $\sigma_\perp$, is negligible, the mean conductivity of a grain, $\sigma_g = \sigma_\perp/3 + 2\sigma_{ab}/3$, is approximated by $\sigma_g \approx 2\sigma_{ab}/3$ whose value is thus between 0.27 and 0.78 S cm^{-1}. This ratio $\sigma_g/\sigma_{ge} \approx 2.7$–$7.8$ obtained from expression (7) corresponds nearly to the interval defined by the values of σ_g/σ_{ge} estimated from expression (6) for the GEM theory. The discrepancy between experimental and calculated dc conductivity values is thus only due to the sample porosity. In the case of a hypothetical small-polaron hopping on nickel sites, the calculated value of σ_g would be between 1.6×10^{-2} and 5×10^{-2} S cm^{-1} at room temperature, obtained by using a concentration N of the lattice sites (3b sites) equal to 2.94×10^{22} cm^{-3}, an occupation ratio f of the nickel 3b site equal to $(1-x)$ and the same values for the other parameters. Consequently, the hypothesis of a small-polaron hopping on nickel sites does not seem realistic, since the σ_g-values are lower than that of the porous medium.

The strength of the relaxation, $\Delta\varepsilon_4$, as a consequence of a small-polaron backward–forward hopping, has an average value of about 56, whatever the temperature is between 220 and 300 K (figure 9). The distribution of the results is due to errors introduced by the CC plot decomposition. This mean value is an effective value while the samples are porous. The determination of the true value of $\Delta\varepsilon_4$ cannot be achieved merely using the GEM theory [47, 48]. Experimental data concerning $\Delta\varepsilon_4$ seem difficult to fully interpret for the moment. However, some remarks can be made in the light of observations made by Bosman and van Daal [17]. The magnitude of $\Delta\varepsilon_4$ cannot be described by a linear dependence on T^{-1} as generally observed in systems in which the corrections due to internal electric fields can be neglected. When the splitting of the energy levels, ΔW, representing the dipoles, is higher than kT, the strength of the relaxation is not dependent on the temperature: the linear dependence on T^{-1} disappears at a temperature $T_0 \approx \Delta W/k$. Briefly, the strength of the relaxation [17, 49] can be approximated as $\Delta\varepsilon \propto m^2/kT$ for $\Delta W < kT$ or $\Delta\varepsilon \propto m^2/\Delta W$ for $\Delta W > kT$.

The bounced-back effect is in fact due to an internal field effect arising from a repulsive coulombic interaction between the polarons. Since ΔW is equal to 0.05 eV for $LiNiO_2$, the linear dependence on T^{-1} would occur from temperature $T_0 \approx 580$ K. Unfortunately, this assumption cannot be verified because the available experimental device is not suitable for measurements above 450 K.

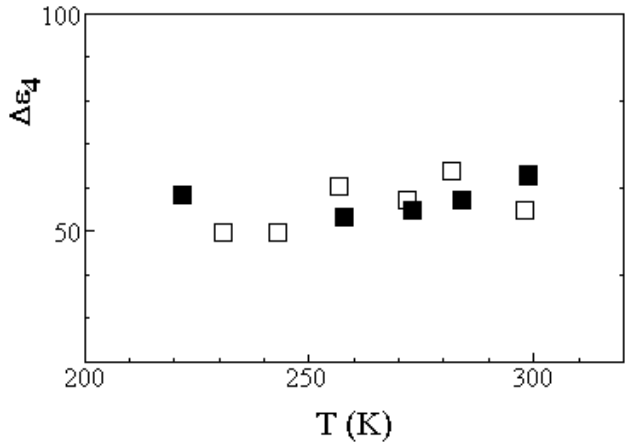

Figure 9. Strength of the relaxation (domain 4) due to small-polaron hopping as a function of the temperature for the samples LNOA (□) and LNOAD (■).

4. Conclusions

Dielectric and conductivity spectroscopy from 10 to 10^{10} Hz has allowed us to determine the electrical transport properties of the granular $Li_{1-x}Ni_{1+x}O_2$ ($x = 0.03$) compound in the temperature range 300–400 K. The interpretation of dielectric and conductivity spectra was made possible through the knowledge of the chemical properties (damaging under air), microstructure and crystalline structure of the samples. The study of the dielectric and conductivity spectra with respect to the sample damaging under air has provided evidence for a transition from a microstructural or interfacial (low-frequency) to a bulk (high-frequency) regime at a crossover frequency ν_{co} in the microwave frequency domain (a few 10^9 Hz at room temperature). For frequencies below ν_{co}, dielectric relaxations were thus attributed to interfacial polarizations as a consequence of the sample microstructures. For frequencies above ν_{co}, a dielectric relaxation attributed to the grain bulk appears. This dielectric relaxation, whose frequency is 8×10^9 Hz at room temperature, is due to thermally activated (hole) small-polaron hopping. However, it is difficult to reach a decision in favour of an adiabatic or a non-adiabatic hopping since the transfer integral J has an experimental value in the region of the phonon frequencies. This ambiguity will be overcome with the knowledge of the experimental value of the LO-phonon frequency in $Li_{1-x}Ni_{1+x}O_2$.

We have shown that dielectric spectroscopy measurements can provide meaningful information regarding the small-polaron dynamics and the influence of the microstructure on the electronic transport in powdered compounds $Li_{1-x}Ni_{1+x}O_2$. Evidence is given that the bulk dc conductivity value of $Li_{1-x}Ni_{1+x}O_2$ is in the range which supports O 2p character of the holes.

From these results, it is clear that the knowledge of the microstructure is of the greatest interest for determining the bulk electrical properties of the materials. Hence, it appears that the only way of determining the electrical properties of granular materials is by using dielectric measurements, over a broad frequency range, from low to microwave frequencies.

Acknowledgment

This work was supported by the Centre National d'Etudes Spatiales (CNES).

References

[1] Reimers J N, Dahn J R, Greedan J E, Stager C V, Liu G, Davidson I and von Sacken U 1993 *J. Solid State Chem.* **102** 542
[2] Yamaura K, Takuno M, Hirano A and Kanno R 1996 *J. Solid State Chem.* **127** 109
[3] Azzoni C B, Paleari A, Massarotti V, Bini M and Capsoni D 1996 *Phys. Rev.* B **53** 703
[4] Barra A L, Chouteau G, Stepanov A, Rougier A and Delmas C 1999 *Eur. Phys. J.* B **7** 551
[5] Li W, Reimers J N and Dahn J R 1992 *Phys. Rev.* B **46** 3236
[6] Ohzuku T, Ueda A, Nagayama N, Iwakoshi Y and Komori H 1993 *Electrochim. Acta* **38** 1159
[7] Broussely M, Perton F, Biensan P, Bodet J M, Labat J, Lecerf A, Delmas C, Rougier A and Pérès J P 1995 *J. Power Sources* **54** 109
[8] Bianchi V, Caurant D, Belhomme C, Chappel E, Chouteau G, Bach S, Pereira-Ramos J P, Sulpice A and Wilmann P 2001 *Solid State Ion.* **140** 1
[9] Kuiper P, Kruizinga G, Ghijsen J, Sawatzky G A and Verweij H 1989 *Phys. Rev. Lett.* **62** 221
[10] Meng J, Jena P and Vail J M 1990 *J. Phys.: Condens. Matter* **2** 10 371
[11] van Elp J, Eskos H, Kuiper P and Sawatzky G A 1992 *Phys. Rev.* B **45** 1612
[12] van Veenandaal M A and Sawatzky G A 1994 *Phys. Rev.* B **50** 11 326
[13] Galakhov V R, Kurmaev E Z, Uhlenbrock St, Neumann M, Kellerman D G and Gorshkov V S 1995 *Solid State Commun.* **95** 347
[14] Harrison N M, Saunders V R, Dovesi R and Mackrodt W C 1998 *Phil. Trans. R. Soc.* A **356** 75
[15] Mizokawa T, Namatame H, Fujimori A, Akayama K, Kondoh H, Kuroda H and Kosugi N 1991 *Phys. Rev. Lett.* **67** 1638
[16] Mackrodt W C 1997 *Ber. Bunsenges. Phys. Chem.* **101** 169
[17] Bosman A J and van Daal A J 1970 *Adv. Phys.* **19** 1
[18] Dutta G, Manthiram A, Goodenough J B and Grenier J C 1992 *J. Solid State Chem.* **96** 123
[19] Lu Zhonghua, Huang Xuejie, Huang Hong, Chen Liquan and Schoonman Joop 1999 *Solid State Ion.* **120** 103
[20] Billig E and Plessner K W 1951 *Proc. Phys. Soc.* B **64** 361
[21] Pecquenard B, Badot J C, Baffier N and Belhadj-Tahar N 1997 *Phys. Status Solidi* a **159** 469
[22] Ragot F, Badot J C, Baffier N and Fourrier-Lamer A 1995 *J. Mater. Chem.* **5** 1155
[23] Lines M E and Glass A M 1979 *Principles and Applications of Ferroelectrics and Related Materials* (Oxford: Clarendon) pp 534–7
[24] Odagaki T, Lax M and Day R S 1992 *Phys. Rev.* B **30** 6911
[25] Fröhlich H 1954 *Adv. Phys.* **3** 325
Fröhlich H 1957 *Arch. Sci.* **10** 5
[26] Iguchi E, Nakamura N and Aoki A 1998 *Phil. Mag.* B **78** 65
[27] Iguchi E, Nakatsugawa H and Futakuchi K 1998 *J. Solid State Chem.* **139** 176
[28] Chern G, Hsieh W K, Tai M F and Hsung K S 1998 *Phys. Rev.* B **58** 1252
[29] Sewell G L 1963 *Phys. Rev.* **129** 597
[30] Mansingh A 1987 Non-Debye relaxation in condensed matter *Proc. Discussion Mtg (Bangalore)* ed T V Ramakrishnan and M Raj Kakshmi (Singapore: World Scientific) p 249
[31] Havriliak S and Negami S 1967 *Polymer* **8** 161
[32] Cole R H and Cole K S 1941 *J. Chem. Phys.* **9** 341
[33] Jonscher A K, Pickup C and Zaidi S H 1986 *Semicond. Sci. Technol.* **1** 71
[34] Lecerf A, Broussely M and Gabano J P 1990 US Patent Specification 4,980,080
[35] Getsinger W J 1966 *IEEE Trans. Microw. Theory Tech.* **14** 58
[36] Kolodziej H and Sobscyk L 1971 *Acta Phys. Pol.* A **39** 59
[37] Badot J C, Fourrier-Lamer A and Baffier N 1985 *J. Physique* **46** 2107
[38] Colomban Ph and Badot J C 1992 *J. Phys.: Condens. Matter* **4** 5625
[39] Ragot F, Badot J C, Baffier N and Fourrier-Lamer A 1998 *Solid State Ion.* **106** 143
[40] Belhadj-Tahar N, Fourrier-Lamer A and de Chanterac H 1990 *IEEE Trans. Microw. Theory Tech.* **38** 1
[41] Jonscher A K 1983 *Dielectric Relaxation in Solids* (London: Chelsea Dielectrics Press)
[42] Funke K 1993 *Prog. Solid State Chem.* **22** 111
[43] Elliott S R 1987 *Adv. Phys.* **36** 135
[44] Holstein T 1959 *Ann. Phys., NY* **8** 343
[45] Alexandrov A S and Mott Sir N 1998 *Polarons and Bipolarons* (Singapore: World Scientific)
[46] Thorn R J 1992 *Physica* C **190** 193
[47] Stauffer D and Aharony A 1992 *Introduction to Percolation Theory* 2nd edn (London: Taylor and Francis)
[48] McLachlan D S 1987 *Solid State Commun.* **60** 821
[49] Mott N F 1990 *Metal–Insulator Transitions* 2nd edn (London: Taylor and Francis)